NUEJ
NARESUAN UNIVERSITY
ENGINEERING JOURNAL

Numerical Solution for Heat and Mass Transfer of Developing Laminar Mixed Convection of Two-Dimensional Inclined Parallel Plates

Sompop Jarungthammachote

Department of Mechanical Engineering, Kasetsart University Sri Racha Campus, Chonburi 20230, E-mail: esrcspj@ku.ac.th

Abstract **– Two-dimensional, developing laminar mixed convection of a binary non-reacting gas mixture flowing in an inclined channel is investigated. A steady state condition is focused through the present study. Thermal boundary conditions of the channel are that one is uniform wall heat flux while the other is uniform wall temperature. Moreover, the walls of channel have different constant species concentrations. The numerical method, called implicit finite difference method, is applied to find hydraulic and heat transfer parameters, consisting of axial and transverse velocities, temperature, and mass fraction. The developments of these parameter profiles, presented in terms of dimensionless form, are observed and discussed. The analytical solution is also presented for fully developed region. The results show that thermal and solutal buoyancy parameters strongly affect on the axial velocity profile. The flow reversal is found near the constant temperature wall for some conditions. If the inclination angle increases, the flow reversal can clearly be observed nearer the inlet of channel. The dimensionless mass fraction, expressing the concentration of focused gas species, and the dimensionless temperature, reflecting the temperature of mixture in the channel, are also interested in this study. The dimensionless mass fraction and the dimensionless temperature profiles continuously change to be linear as distance along the flow direction increase. Based on the condition in this study, the dimensionless mass fraction profile can reach the fully developed condition faster than the dimensionless axial velocity and the dimensionless temperature profiles.**

Keywords – Laminar mixed convection, Developing flow, Flow reversal, Asymmetric boundary condition

1. NOMENCLATURE

D_{AB}	Species diffusion coefficient (m^2/s)
L	Spacing between channel (m)
Gr_C	Solutal Grashof number, $Gr_C = g\zeta\left(\omega_2 - \omega_1\right)L^3/\nu^2$ (-)
Gr_T	Thermal Grashof number, $Gr_T = g\beta q'' L^4/k\nu^2$ (-)
k	Thermal conductivity (W/m·K)
p	Pressure (Pa)
P	Dimensionless pressure (-)
Pr	Prandtl number (-)
q''	Heat flux (W)
r_M	Mass fraction ratio (-)
$\bar{R}$	Universal gas constant, 8.3145 (kJ/kmol·K)
Re	Reynolds number (-)
Sc	Schmidt number (-)
T	Temperature (K)
u	Axial velocity (m/s)
v	Transverse velocity (m/s)
U	Dimensionless axial velocity (-)
V	Dimensionless transverse velocity (-)
W	Dimensionless mass fraction (-)
x, y	Cartesian coordinates (m)
X, Y	Dimensionless coordinates (-)

Greek letters

α	Thermal diffusivity (m^2/s)
β	Thermal expansion coefficient (1/K)
ζ	Solutal expansion coefficient (-)
γ	Inclination angle of channel (^{o})
ν	Kinematic viscosity (m^2/s)
θ	Dimensionless temperature (-)
ρ	Density (kg/m^3)
ω	Mass fraction of diffusing species (-)

Subscripts

1	Uniform heat flux wall of channel
2	Constant temperature wall of channel
o	Free stream value

2. INTRODUCTION

Many natural phenomena and industrial thermal processes influence of a coupled heat and mass transfer mechanism. Researchers are, therefore, interested to study this process in various issues. The analyses of convection with or without mass transfer in parallel-plate channel are interesting and found in the literatures. The exact solution of fully developed mixed convection in a parallel-plate vertical channel was found by Aung and Worku [1]. The forced flow entering the channel is in the vertical upward direction. The boundary conditions of this problem are defined as asymmetric uniform temperatures. Barletta and Zanchini [2] studied a similar problem, but different thermal boundary conditions. The aim of their study is to investigate the effect of the choice of the reference fluid temperature on the solution of problem. The effect of combined buoyancy force of thermal and mass diffusions on turbulent forced convection heat and mass transfer was numerically examined by Yan [3]. Low-Reynolds-number $k-\varepsilon$ model was used to solve the problem. The thermal boundary conditions, considered in his study, are the first and second type symmetrical wall thermal conditions. The researcher found that opposing-buoyancy forces caused an enhancement in turbulent heat and mass transfer. Lee et al. [4] investigated mixed convection heat and mass transfer in a vertical rectangular duct with film evaporation along the porous wall by using a numerical method. The fluid considered in their study is moist air. The numerical result presented that the effects of film evaporation along the vertical wall on the Nusselt number is significant. Belhadj Mohamed et al. [5] numerically analyzed a problem of condensation by mixed convection in a vertical channel for air-water system. The Soret and Duffour effects were negligible. In the energy equation, the radiation heat transfer and the viscous dissipation were neglected to include. The axial velocity, concentration, and temperature profiles were obtained. The sensible and latent Nusselt numbers were also observed along the channel. A problem of laminar mixed convection between vertical parallel plates was numerically studied by Salah El-Din [6]. A binary gas mixture flowed upward into a channel and the walls of channel were set to have different uniform heat and mass fluxes. The velocity, temperature, concentration profiles as well as pressure gradient were focused. The effect of the buoyancy ratio (the ratio of mass Grashof number and Grashof number) on the local Nusselt number and Sherwood number was observed. The calculation result showed that the positive buoyancy ratio increased Nusselt and Sherwood numbers while negative buoyancy ratio decreased them. An analytical solution for fully developed mixed convection between parallel vertical plates with heat and mass transfer was found by Boulama and Galanis [7]. The boundary conditions of isothermal walls and uniform wall heat fluxs were considered in the study. The exact solutions of dimensionless temperature, mass fraction, axial velocity, and pressure gradient for both cases of boundary conditions were provided in the study. Lately, Boulama et al. [8] extended the previous study to inclined parallel-plate channel. The effects of thermal and solutal buoyancy parameters as well as inclination angle on the dimensionless temperature, mass fraction, axial velocity, Nusselt and Sherwood numbers were exhibited. A study of mixed convection in a vertical parallel-plate channel with evaporation of thin liquid films on wetted walls was conducted by Laaroussi et al. [9]. Air-water vapor and air-hexane were applied in the study and these gases flowed downward into the channel. The effect of variable density was focused and a commercial program was used to simulate the behavior of the system. The authors discussed that the Boussinesq approximation provides the result, which is different from fully variable property model. A similar mathematical model, used in Ref. [9], was found to be used in Ref. [10]. However, the study was concentrated on the investigation of flow reversal.

To the author's best knowledge, there are a few works studying on the laminar mixed convection in an inclined parallel-plate channel with heat and mass transfer, especially developing region. Moreover, the boundary conditions are usually symmetry. In this study, two-dimensional, laminar mixed convection in developing region with combined uniform heat flux and constant temperature boundary conditions is study through numerical method. The developments of axial velocity, temperature, and mass fraction profiles are focused. The effects of inclination angle as well as the thermal and solutal buoyancy parameters on these profiles are also investigated.

3. DESCRIPTION AND FORMULATION OF THE PROBLEM

A two-dimensional steady-state laminar flow between inclined parallel plates is considered in this study. The plates are separated by distance L and both are oriented at an angle γ to the horizontal, as shown in Fig. 1.

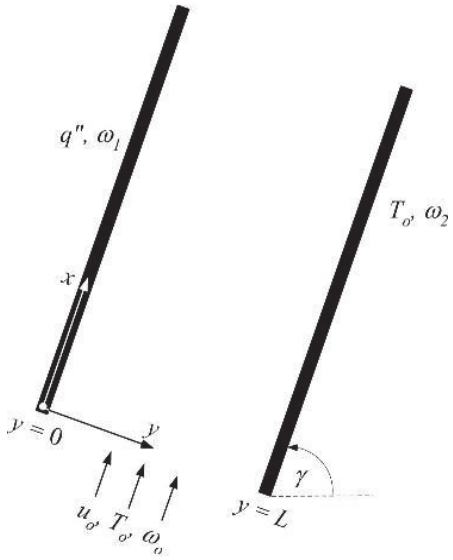

Figure 1 Schematic representation of physical problem

In the channel, fluid is a mixture of two non-reacting gases consisting of a large quantity of gas A and a small quantity of gas B. The fluid enters the channel with a uniform

velocity distribution u_o, constant temperature T_o, and uniform concentration ω_o, defined as the ratio of mass of gas B per total mass. The coordinate system is chosen such that the x-axis lies on the axial plane of the channel and the y-axis is orthogonal to the walls. The origin of the axes is positioned on the wall, numbered by 1. The gravitational acceleration points downward. The effects of concentration gradient on the thermal diffusion (Dufour effect) and thermal gradient on the mass diffusion (Soret effect) are not considered in this study. The themophysical properties of fluid are assumed to be constant except for the density in the body forces, which is considered to be a linear function of temperature and mass fraction, obeying Boussinesq approximation. The viscous dissipation, radiation heat transfer, and the internal heat generation are neglected in this analysis. According to the above assumptions, the governing equations of the problem can be written as:

Continuity equation

$$\frac{\partial u}{\partial x}+\frac{\partial v}{\partial y}=0 \tag{1}$$

x-momentum equation

$$u\frac{\partial u}{\partial x}+v\frac{\partial u}{\partial y}=-\frac{1}{\rho}\frac{\partial p}{\partial x}+\nu\left(\frac{\partial^2 u}{\partial y^2}\right)+g\beta\left(T-T_o\right)\sin\gamma+ g\zeta\left(\omega-\omega_o\right)\sin\gamma \tag{2}$$

Energy equation

$$u\frac{\partial T}{\partial x}+v\frac{\partial T}{\partial y}=\alpha\frac{\partial^2 T}{\partial y^2} \tag{3}$$

Species conservation equation

$$u\frac{\partial \omega}{\partial x}+v\frac{\partial \omega}{\partial y}=D_{AB}\frac{\partial^2 \omega}{\partial y^2} \tag{4}$$

Introducing the following dimensionless quantities,

$$U=\frac{u}{u_o},\quad V=\frac{vRe}{u_o},\qquad X=\frac{x}{ReL},\quad Y=\frac{y}{L},$$
$$P=\frac{p}{\rho u_o^2},\quad W=\frac{\omega-\omega_o}{\omega_1-\omega_o},\quad \theta=\frac{\left(T-T_o\right)k}{q"L}$$

Eqs. (1)-(4) can be rewritten, respectively, in the dimensionless form as:

$$\frac{\partial U}{\partial X}+\frac{\partial V}{\partial Y}=0 \tag{5}$$

$$U\frac{\partial U}{\partial X}+V\frac{\partial U}{\partial Y}=-\frac{dP}{dX}+\frac{\partial^2 U}{\partial Y^2}+\frac{Gr_T}{Re}\theta\cdot\sin\gamma+ \frac{Gr_C}{Re}W\cdot\sin\gamma=0 \tag{6}$$

$$U\frac{\partial \theta}{\partial X}+V\frac{\partial \theta}{\partial Y}=\frac{1}{Pr}\frac{\partial^2\theta}{\partial Y^2} \tag{7}$$

$$U\frac{\partial W}{\partial X}+V\frac{\partial W}{\partial Y}=\frac{1}{Sc}\frac{\partial^2 W}{\partial Y^2} \tag{8}$$

These equations are subjected to the following boundary conditions:

At inlet $\left(X=0\right)$: $U=1$ and $V=\omega=\theta=0$ (9a)

At the wall 1 $\left(Y=0\right)$: $U=V=0$, $W=1$, and,

$$\left(\frac{\partial\theta}{\partial Y}\right)=-1 \tag{9b}$$

At the wall 2 $\left(Y=1\right)$: $U=V=\theta=0$ and

$$W=r_M=\frac{\omega_2-\omega_o}{\omega_1-\omega_o} \tag{9c}$$

From Eq. (9b), it can be observed that the slope of the dimensionless temperature is negative. It means the temperature decreases from left to right. Moreover, at Y=1, $\theta=1$, it expresses that the temperature on the constant temperature wall is not raised. From both boundary conditions, it can be implied that the temperature on the uniform heat flux wall is higher than that on the constant temperature wall.

4. NUMERICAL SOLUTION

In this study, the developing flow region is mainly focused. The fully developed flow, however, will also be discussed. The analytical solutions to the governing equations, expressed in previous section, are difficult to obtain. Therefore, the numerical technique, called implicit finite difference scheme, is employed. The space grid, used in the calculation, is shown in Fig. 2. The grid points have coordinates $X=i\Delta X$ and $Y=j\Delta Y$ where *i* and *j* are grid indices in the flow and transverse directions, respectively. The details involving with setting of ΔX and ΔY will be mentioned in further section. The finite difference form of the dimensionless governing equations can be written as follows:

Continuity equation:

$$\frac{U_{(i+1,j)}+U_{(i+1,j-1)}-U_{(i,j)}-U_{(i,j-1)}}{2\Delta X}+\frac{V_{(i+1,j)}-V_{(i+1,j-1)}}{\Delta Y}=0 \tag{10}$$

x-momentum equation

$$U_{(i,j)}\left(\frac{U_{(i+1,j)}-U_{(i,j)}}{\Delta X}\right)+V_{(i,j)}\left(\frac{U_{(i+1,j+1)}-U_{(i+1,j-1)}}{2\Delta Y}\right)=$$
$$\frac{P_{(i+1,j)}-P_{(i,j)}}{\Delta X}+\left(\frac{U_{(i+1,j+1)}-2U_{(i+1,j)}+U_{(i+1,j-1)}}{\Delta Y^2}\right)+ \quad (11)$$
$$\frac{Gr_T}{Re}\theta_{(i+1,j)}(\sin\gamma)+\frac{Gr_C}{Re}W_{(i+1,j)}(\sin\gamma)$$

Energy equation

$$U_{(i,j)}\left(\frac{\theta_{(i+1,j)}-\theta_{(i,j)}}{\Delta X}\right)+V_{(i,j)}\left(\frac{\theta_{(i+1,j+1)}-\theta_{(i+1,j-1)}}{2\Delta Y}\right)=$$
$$\frac{1}{Pr}\left(\frac{\theta_{(i+1,j+1)}-2\theta_{(i+1,j)}+\theta_{(i+1,j-1)}}{\Delta Y^2}\right) \quad (12)$$

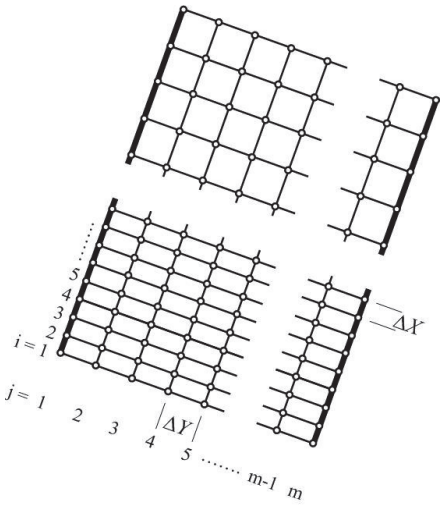

Figure 2 The grid points used in numerical calculation

For species conservation equation, the finite difference formulation can be developed in the similar way as Eq. (12).

To find the dimensionless velocity components, temperature, mass fraction, and pressure distributions, some parameters, for instance, Gr_T / Re, $Gr_C / Re, Pr$, and Sc, should be firstly assigned the values. The inlet boundary conditions are set. The thermal and hydrodynamic boundary conditions are given for the nodes on the walls. The temperatures at cross section of i+1, expressed in the energy equation, are initially solved. This equation uses the velocity components and temperature from the previous cross section (i). For example, at i+1=2, the temperatures at this cross section can be found using the velocity and temperature values at i=1 (inlet boundary condition). Considering Eq. (12), it can be arranged in tri-diagonal matrix. A numerical method, for instance Gauss elimination method, is probably applied to obtain the solution with relative convergence criterion of 1×10^{-5}. The species conservation equation is, then, solved. However, it has no effect if this equation is solved before solving energy equation. In the next step, the dimensionless axial velocity component and dimensionless pressure are obtained by calculating the x-momentum equation. The dimensionless temperature and mass fraction from the previous step are substituted into Eq. (11). The dimensionless velocity components from previous cross section (i) are also used. A tri-diagonal matrix is formed and a numerical method is used to find the dimensionless axial velocity at cross section i+1. To obtain the dimensionless transverse velocity component, the axial velocity component, obtained from the previous step, is substituted into Eq. (10). At j=2, the transverse velocity at node j-1 is given by hydrodynamic boundary condition. Thus, $V_{(i+1,j)}$ can be finally found. For calculation of variables (θ, W, U, V, P) at the next cross section, the above procedures are repeated until the fully developed condition is achieved.

5. ANALYSIS FOR FULLY DEVELOPED SOLUTION

Considering the problem, if the channel is sufficiently long, the axial velocity, temperature, and concentration profiles can be assumed to be independent of the distance along the channel. The governing equations, presented in dimensionless form, can be written as:

$$-\frac{dP}{dX}+\frac{\partial^2 U}{\partial Y^2}+\frac{Gr_T}{Re}\theta\cdot\sin\gamma+\frac{Gr_C}{Re}W\cdot\sin\gamma=0 \quad (13)$$

$$\frac{\partial^2\theta}{\partial Y^2}=0 \quad (14)$$

$$\frac{\partial^2 W}{\partial Y^2}=0 \quad (15)$$

Solving the dimensionless temperature and species mass fraction equations with the boundary conditions and substituting the results into Eq. (13), the dimensionless axial velocity can be solved and the solution is:

$$U(Y)=-\frac{Gr_T}{Re}\sin\gamma\left(-\frac{Y^3}{6}+\frac{Y^2}{2}-\frac{Y}{3}\right)-$$
$$\frac{Gr_C}{Re}\sin\gamma\left[(r_M-1)\left(\frac{Y^3}{6}-\frac{Y}{6}\right)+\frac{Y^2}{2}-\frac{Y}{2}\right]+\frac{dP}{dX}\left(\frac{Y^2}{2}-\frac{Y}{2}\right) \quad (16)$$

To find the pressure gradient, dP/dX, the mass flow rate per unit width, expressed in Eq. (17) [11], is introduced:

$$\int_0^1 U dY=1 \quad (17)$$

Finally, the equation described pressure gradient is:

$$\frac{dP}{dX}=-12+\frac{Gr_T}{Re}\frac{\sin\gamma}{2}+\frac{Gr_C}{Re}\sin\gamma\left(\frac{(r_M-1)}{2}+1\right) \quad (18)$$

Substituting Eq. (18) into Eq. (16), one can write the dimensionless axial velocity as:

$$U(Y)=\left(\frac{-Gr_T+Gr_C(r_M-1)}{Re}\right)\sin\gamma\left(\frac{-2Y^3+3Y^2-Y}{12}\right)+6\left(-Y^2+Y\right) \quad (19)$$

From Eq. (18), if the thermal and solutal buoyancy effects are disappear ($Gr_T=Gr_C=0$) (only forced convection), the dimensionless pressure gradient is equal to -12. This has been confirmed by Salah El-Din [6]. Moreover, in the analytical result of combined convection, presented in [11], it also provided the same result of dimensionless pressure gradient if buoyancy force is negligible. For Eq. (19), it is worth to noting here that in the forced convection case $\left(Gr_T=Gr_C=0\right)$, the velocity profile in Eq. (19) is reduced to

$$U(Y)=6\left(-Y^2+Y\right) \quad (20)$$

which is identical to that was mentioned in Oosthuizen and Naylor [11] and Grosan et al. [12].

6. VALIDATION

To validate the numerical result, the computation by finite difference method is carried out from X = 0 to a certain value of X, which is expected to reach the fully developed flow. The numerical result of dimensionless axial velocity is, then, compared with that calculated from Eq. (19). The validation procedure was started with setting the value of X at which the fully developed flow should be satisfied. The dimensionless axial velocity was computed following the finite difference technique. If the different values of velocity in the last step (at X) and the previous step (at $X-\Delta X$), compared at the same node, are averagely less than 0.1%, the section at X is considered to be in fully developed flow region and the dimensionless axial velocity profile is compared with that from analytical method in order to validate the result. Moreover, the variations of dimensionless temperature and species mass fraction are also investigated to make sure that the numerical results agree with the solutions of Eqs. (14) and (15). However, if the dimensionless axial velocity obviously varies from section to section, the value of X will be increased and calculation will be carried out again. The values of parameters used in this section are listed in Table 1 and the validation result is elucidated in Fig. 3.

From Fig. 3, it expresses that the dimensionless axial velocity profile calculated from numerical method with X =1.5 matches with that from analytical equation, Eq. (19). It implies that the numerical method, explained in previous section, can provide reasonably accurate results. The divergence between both methods can be noticed at peak and flow reversal regions. Moreover, the numerical result at X = 2.5 is also exhibited in Fig. 3. It can be clearly observed that the result from numerical method is completely identical with that from analytical method. However, it is worth to mention here that after X = 0.5, the velocity profile is slightly change or it approaches fully developed region. To save the computational time, the value of ΔX beyond X = 0.5 can be increased, as shown in Fig. 2. The other parameter used in the validation is the dimensionless pressure gradient. As mentioned in the previous section, if the thermal and solutal buoyancy effects are neglected $\left(Gr_T/Re=Gr_C/Re=0\right)$ the dimensionless pressure gradient is equal to -12. The pressure gradient of -12 has been performed to confirm the accuracy and convergence of the numerical computations in Salah El-Din [6]. At X = 1.5, the dimensionless pressure gradient from numerical method is -12.030 for $\Delta Y=5\times10^{-2}$ and it is equal to -12.004 for $\Delta Y=2\times10^{-2}$. Thus, the above validations confirm that the numerical method, developed in this study, gives the reasonably accurate results.

Table 1 Parameter values used in the validation

Parameter	Value
Gr_T/Re	130
Gr_C/Re	15
Pr	0.7
Sc	0.68
γ	60°
X	1.5, 2.5
ΔX	5×10^{-3}
ΔY	5×10^{-2}
r_M	1.5

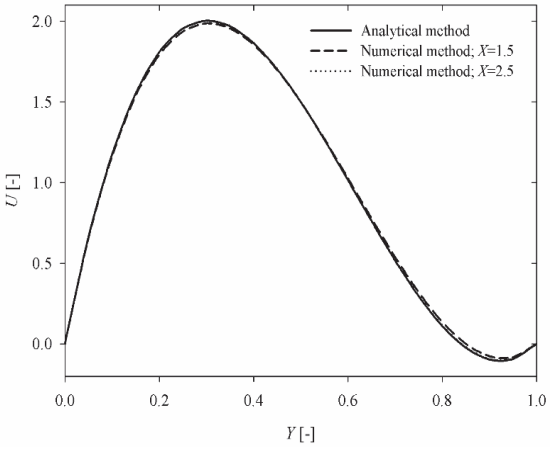

Figure 3 Comparison of dimensional axial velocity obtained from analytical and numerical method

7. RESULTS AND DISCUSSION

In this section, the variations of axial velocity, temperature, and concentration profiles in the channel are shown. For the dimensionless transverse velocity, V, is not considered in this study, because it has low magnitude when compared with the dimensionless axial velocity. The numerical calculations performed here use the parameter values previously listed in Table 1, except ΔY and γ . In order to

obtained the accuracy result compromised with the consumption of computer resources, the grid sensitivity was tested and the value of ΔY accepted for the calculation is 2×10^{-2}.

Fig. 4 shows the dimensionless axial velocity profiles of the fluid in the channel, which is rotated at 45° to the horizontal. The profiles are computed for different values of X. At $X = 0.05$, the velocity profile is quit symmetric. It can be implied that the effects of buoyancy forces are small. This is confirmed by the shape of dimensionless velocity profile described by Eq. (20). As X increases, the velocity profile develops and the non-symmetrical shape is clearly observed. At $X = 0.5$, the absolute value of the profile slope at the constant temperature wall is small and almost becomes zero while the velocity near the uniform heat flux wall is accelerated due to the thermal buoyancy force. Another interesting topic, which should be pointed out here, is the effects of thermal and solutal buoyancy forces on the velocity profile. In section 2, the boundary conditions describe that the temperature of the uniform heat flux wall should be higher than that of the constant temperature wall. Therefore, the thermal buoyancy force near this wall should also be stronger. However, the concentration of species B at the constant temperature wall has higher value than that at the uniform heat flux wall. Then, the effect of solutal buoyancy force near the constant temperature wall is meaningful. The effects of both buoyancy forces, which show their significances in different sides, cause solutal and thermal Grashof numbers presented in Eq. (19) having different signs (for this study,

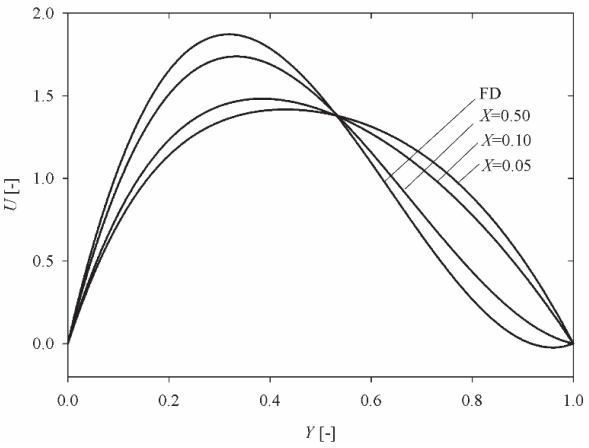

Figure 4 Dimensionless axial velocity profiles for different values of X with $\gamma = 45^o$, $Gr_T/Re = 130$, $Gr_C/Re = 15$ and FD=fully developed condition

r_M is higher than 1). However, it should be noticed in Table 1 that the value of the thermal buoyancy parameter, Gr_T/Re, is higher than the value of the solutal buoyancy parameter, Gr_C/Re. Therefore, the effect of the thermal buoyancy force contributes to the acceleration of velocity more than that of solutal buoyancy force. The velocity near the uniform heat flux is increased. Because of the conservation of total mass flow rate at any cross section, the flow deceleration takes place near the constant temperature wall. The dimensionless velocity profile at fully developed region (X = 2.5), indicated by the letters FD, is also expressed to compare with the velocity profiles in developing region. It reveals the flow reversal happening near the constant temperature wall.

Fig. 5 shows the variation of dimensionless axial velocity with Y at different values of inclination angle, γ. All profiles are at $X = 0.5$. From the figure, it can be noted that the dimensionless velocity near the uniform heat flux wall continuously increases with increasing inclination angle of the channel. However, the contrast phenomena can be noticed near the constant temperature wall. The dimensionless velocity clearly decelerates and the flow reversal can be detected when inclination angle is higher than 60°. This can be explained that the thermal buoyancy effect has more impact on the dimensionless velocity than the solutal buoyancy effect, indicated by the thermal buoyancy parameter which is higher than the solutal buoyancy parameter. The velocity near the uniform heat flux wall is, then, accelerated when the inclination angle of the channel increases. However, the total mass flow rate at any cross section of the channel is conserved. Thus, the dimensionless velocity near the constant temperature wall decreases. Therefore, it is continuously distorted as the inclination angle enlarges.

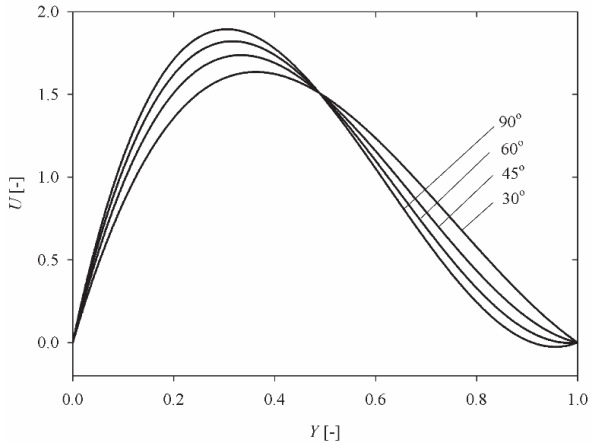

Figure 5 Dimensionless axial velocity profiles for different values of γ with $X = 0.5$, $Gr_T/Re = 130$, $Gr_C/Re = 15$

Another topic, discussed here, is the criterion of flow reversal. The flow starts to reverse the direction when $dU/dY = 0$. For fully developed flow, the flow reversal can be exactly analyzed from Eq. (16) that it will occur when $\left(-Gr_T + Gr_M\left(r_M - 1\right)\right)\sin(\gamma)/Re < -72$. If Gr_T, Gr_M, r_M, and Re are defined, the inclination angle, at which the flow starts to reverse, can be found. Fig. 6 illustrates the dimensionless axial velocity along the channel from $X = 0$ to $X = 2.5$ with contour lines. The dimensionless velocity are computed with $\gamma = 60^o$. The figure clearly indicates

that the flow reversal takes place after X=0.5 (see the dash line). This is the same case showed in Fig. 5 with $\gamma = 60^o$.

Note that, for the dimensionless transverse velocity profile, its magnitude is less than the magnitude of the dimensionless axial velocity at the same X. Thus, it is not focused here. However, from the calculation, the dimensionless transverse velocity continuously reduces and it is about zero at fully developed region.

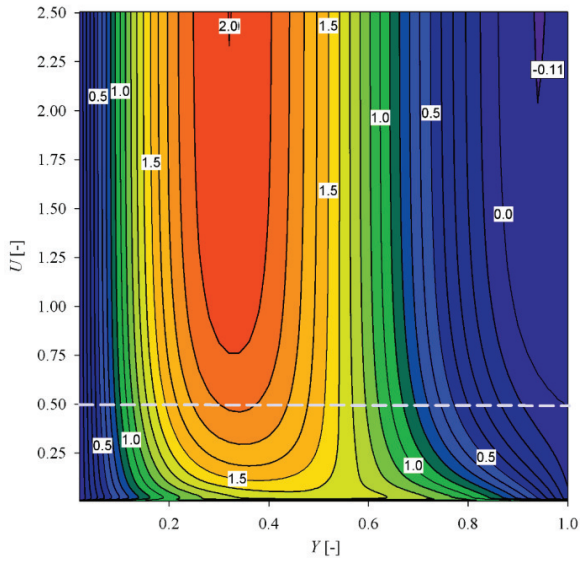

Figure 6 Dimensionless axial velocity along the channel and contour lines with $\gamma = 60^o$, $Gr_T/Re = 130$, $Gr_C/Re = 15$

Fig. 7 shows the dimensionless temperature profiles at different values of X. The dimensionless temperature on the wall increases, associated with the boundary condition of constant heat flux, while the dimensionless temperature on the constant temperature wall is fixed at zero. At small X, the dimensionless temperature profile is nonlinear and it finally adjusts to be a linear relation with Y at fully developed region. This can be proved by solving Eq. (14) with boundary conditions. It gives the dimensionless temperature profile as $\theta(Y)=1-Y$ which is linear relationship with Y.

The dimensionless mass fraction profiles at different values of X are shown in Fig. 8. The profile is parabolic shape at small X and it continuously changes to be linear when X increases. It can also be proved by solving Eq. (15) with boundary conditions and it finally expresses that $W(Y)=1+(r_M-1)Y$. It clearly presents that at fully developed condition, the dimensionless mass fraction is linear relationship with Y.

Comparing to the dimensionless axial velocity and temperature profiles, the dimensionless mass fraction profile can reach the fully developed condition faster than others. As found in Fig. 8, the profile of mass fraction at X = 0.5 coincides with that at the fully developed region. However, the different value of both profiles is possibly to be observed. Therefore, it can be mentioned that, beyond X = 0.5, the variation of dimensionless mass fraction with X or $\partial W/\partial X$ is about zero.

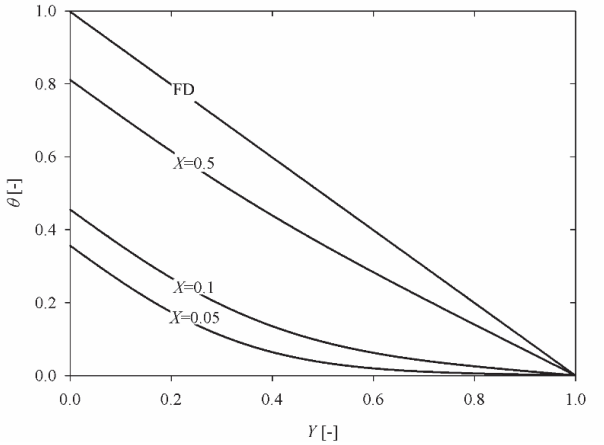

Figure 7 Dimensionless temperature profiles for different values of X with $\gamma = 60^o$, $Gr_T/Re = 130$, $Gr_C/Re = 15$

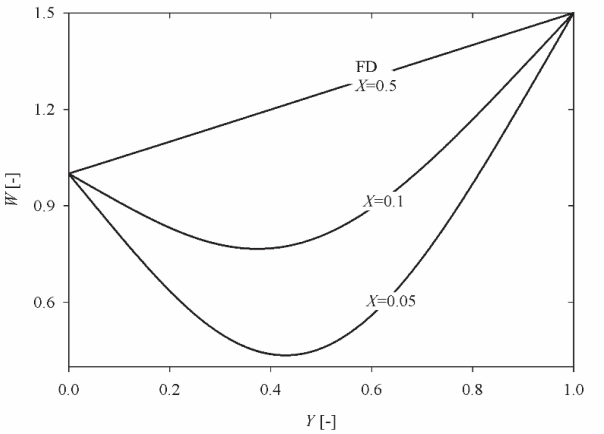

Figure 8 Dimensionless mass fraction profiles for different values of X with $\gamma = 60^o$, $Gr_T/Re = 130$, $Gr_C/Re = 15$

For the effects of inclination angle, γ, on the temperature and mass fraction profiles, γ at 30º, 45º, 60º, and 90º are used to find temperature and mass fraction. Figs. 9 and 10 indicate that the dimensionless temperature and mass fraction profiles at different values of γ are almost completely coincidental. Small figures are added in order to clearly see the profiles. The increase of γ from 30º to 60º causes 4.3% of the maximum change of θ and 2.6% of the maximum change of W. It can be observed that in Eq. (12), used to find the dimensionless temperature, no inclination angle, γ, appears. However, the inclination angle affects the axial velocity, which is found in Eq. (12). Thus, the inclination angle indirectly influences on the temperature profile. The same explanation can be used for the mass fraction profile.

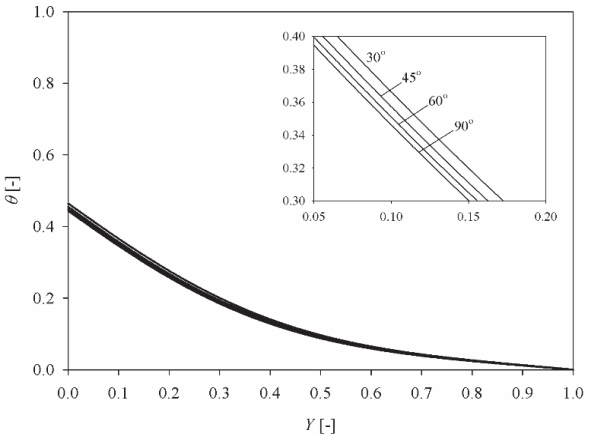

Figure 9 Dimensionless temperature profiles for different values of γ with $X = 0.5$, $Gr_T/Re = 130$, $Gr_C/Re = 15$

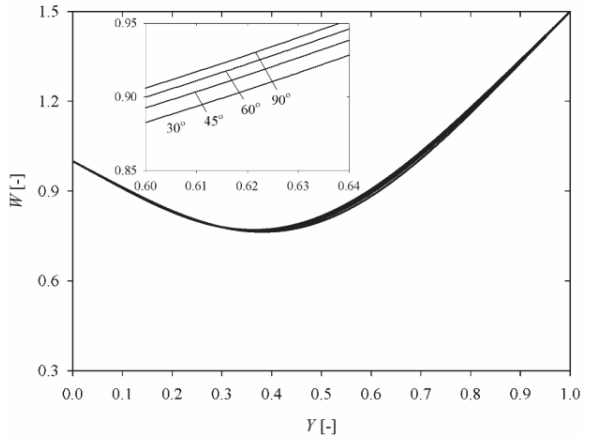

Figure 10 Dimensionless mass fraction profiles for different values of γ with $X = 0.5$, $Gr_T/Re = 130$, $Gr_C/Re = 15$

8. CONCLUSION

The developing laminar mixed convection with heat and mass transfer between inclined parallel plates has been studied numerically. The first plate supplies constant heat flux and the other is fixed at constant temperature. It is found that the dimensionless axial velocity is strongly dependent on the thermal and the solutal buoyancy parameters as well as inclination angle of the channel. Due to higher thermal Grashof number, the reversal flow may be found near the constant temperature wall at the location far from inlet of channel. It, however, also depends on other parameters, for example inclination angle. Higher inclination angle can cause reversal flow at earlier length of channel. The dimensionless temperature and mass fraction profiles continuously develop and become linear profiles at fully develop region. Compared to the dimensionless axial velocity profile, the dimensionless temperature and mass fraction profiles are slightly affected by the inclination angle.

9. REFERENCES

[1] W. Aung and G. Worku, "Theory of fully developed, combined convection including flow reversal," *J. Heat Transfer*, vol. 108, pp.485-488, 1986.

[2] A. Barletta and E. Zanchini, "On the choice of the reference temperature for fully-developed mixed convection in a vertical channel," *Int. J Heat Mass Transfer*, vol. 42, pp. 3169-3181, 1999.

[3] W.M Yan, "Effects of film vaporization on turbulent mixed convection heat and mass transfer in a vertical channel," *Int. J. Heat Mass Transfer*, vol. 38, pp. 713-722, 1995.

[4] K.T. Lee, H.L. Tsai, and W.M. Yan, "Mixed convection heat and mass transfer in vertical rectangular ducts," *Int. J. Heat Mass Transfer*, vol. 40, pp.1621-1631, 1997.

[5] A. Belhadj Mohamed, J. Orfi, A. Debbissi, and S. Ben Nasrallah, "Heat and mass transfer during condensation in a vertical channel under mixed convection," *Heat Mass Transfer*, vol. 43, pp. 851-861, 2007.

[6] M.M. Salah El-Din, "Effect of thermal and mass buoyancy forces on the development of laminar mixed convection between vertical parallel plates with uniform wall heat and mass fluxes," *Int. J. Therm Sci.,* vol. 42, pp. 447-453, 2003.

[7] K. Boulama and N. Galanis, "Analytical solution for fully developed mixed convection between parallel vertical plates with heat and mass transfer," J. *Heat Transfer-Trans ASME*, vol. 126, pp. 381-388, 2004.

[8] K. Boulama, N. Galanis, and J. Orfi, "Thermosolutal mixed convection and flow-reversal in an inclined parallel-plate channel," *Heat Mass Tranfer*, vol. 48, pp. 1601-1613, 2012.

[9] N. Laaroussi, G. Lauriat, and G. Desrayaud, "Effects of variable density for film evaporation on laminar mixed convection in a vertical channel," *Int. J. Heat Mass Transfer*, vol. 52, pp. 151-164, 2009.

[10] O. Oulaid, B. Benhammou, and N. Galanis, "Flow reversal in combined laminar mixed convection heat and mass transfer with phase change in a vertical channel," Int. J. Heat Fluid Flow, vol. 31, pp. 711-721, 2010.

[11] P.H. Oosthuizen and D. Naylor, *An introduction to convective heat transfer analysis*, McGraw-Hill; 1999.

[12] T. Grosan, R. Pop, and I. Pop, "Thermophoretic deposition of particles in fully developed mixed convection flow in a parallel-plate vertical channel," *Heat Mass Transfer* , vol. 45, pp. 503-509, 2009.